

J. C. M. de Hoog · K. H. Hattori · R. P. Hoblitt

Oxidized sulfur-rich mafic magma at Mount Pinatubo, Philippines

Received: 16 January 2003 / Accepted: 21 October 2003 / Published online: 22 November 2003
© Springer-Verlag 2003

Abstract Basaltic fragments enclosed in andesitic dome lavas and pyroclastic flows erupted during the early stages of the 1991 eruption of Mount Pinatubo, Philippines, contain amphiboles that crystallized during the injection of mafic magma into a dacitic magma body. The amphiboles contain abundant melt inclusions, which recorded the mixing of andesitic melt in the mafic magma and rhyolitic melt in the dacitic magma. The least evolved melt inclusions have high sulfur contents (up to 1,700 ppm) mostly as SO_4^{2-} , which suggests an oxidized state of the magma (NNO + 1.4). The intrinsically oxidized nature of the mafic magma is confirmed by spinel–olivine oxygen barometry. The value is comparable to that of the dacitic magma (NNO + 1.6). Hence, models invoking mixing as a means of releasing sulfur from the melt are not applicable to Pinatubo. Instead, the oxidized state of the dacitic magma likely reflects that of parental mafic magma and the source region in the sub-arc mantle. Our results fit a model in which long-lived SO_2 discharge from underplated mafic magma accumulated in the overlying dacitic magma and immiscible aqueous fluids. The fluids were the most likely source of sulfur that was released into the atmosphere during the cataclysmic eruption. The concurrence of highly oxidized basaltic magma and disproportionate sulfur output during the 1991 Mt. Pinatubo eruption suggests that oxidized mafic melt is an efficient medium for transferring sulfur from the mantle to shallow crustal levels and the atmosphere. As it can carry large amounts of sulfur, effectively scavenge sulfides from the source

mantle and discharge SO_2 during ascent, oxidized mafic magma forms arc volcanoes with high sulfur fluxes, and potentially contributes to the formation of metallic sulfide deposits.

Introduction

The cataclysmic eruption of Mount Pinatubo on 15 June 1991, was preceded by the extrusion of dome-forming andesite and discharge of andesitic scoria. These andesitic rocks are a product of magma mixing during the injection of basaltic magma into the shallow dacitic magma reservoir, which may also have triggered the eruption (Pallister et al. 1996). The eruption injected at least 17 Mt SO_2 into the stratosphere (Self et al. 1996). The eruption products were unusually sulfur-rich with bulk contents of 1,500–2,400 ppm S, and contained anhydrite phenocrysts (Pallister et al. 1992; Bernard et al. 1996). Furthermore, the dacitic magma contained an exsolved aqueous fluid phase that was rich in sulfur and provided the SO_2 discharged to the atmosphere (Westrich and Gerlach 1992; Gerlach et al. 1996; Hattori 1996; Scaillet and Evans 1999).

What caused the enrichment of sulfur in the aqueous phase and dacitic magma is in debate. Proposed opinions include assimilation of sulfur-bearing alteration minerals (McKibben et al. 1992; Rutherford and Devine 1996) and degassing of underlying basaltic magma (Pallister et al. 1992, 1996; Hattori 1993, 1996; Gerlach et al. 1996). Alternatively, sulfur could be derived from mixing between anhydrite-saturated dacite and sulfide-saturated basalt, a process that would force both sulfur-bearing phases out of their stability field and drive sulfur out of the magma (Matthews et al. 1992; Kress 1997). A pivotal role for basaltic magma is envisaged in most of these scenarios, but, so far, little direct evidence has been presented, in part because basaltic fragments are scarce. The limited evidence from basaltic fragments in dome-forming andesite suggested that the mafic magma might

Editorial responsibility: J. Hoefs

J. C. M. de Hoog (✉)
Dept. of Earth Sciences, Gothenburg University,
413 20 Göteborg, Sweden
E-mail: cees-jan@gvc.gu.se

J. C. M. de Hoog · K. H. Hattori
Dept. of Earth Sciences, University of Ottawa, Ottawa,
ON, K1N 6N5, Canada

R. P. Hoblitt
US Geological Survey, Hawaii National Park, HI 96718, USA

have been sulfur-rich and reduced because of the presence of sulfide globules (Hattori 1993, 1996). This paper documents the compositions of minerals and melt inclusions in the basaltic fragments in order to characterize the role of primitive magma in the events at Pinatubo and its significance for the origin of oxidized felsic arc magmas.

Geological background and eruption history

Mount Pinatubo is a part of the Luzon arc (Fig. 1), whose volcanism is related to the eastward subduction of the South China Sea Plate along the Manila Trench. Pinatubo is a stratovolcano consisting of dacitic pyroclastic-flow and lahar deposits, and is underlain by gabbroic and ultramafic rocks of the Zambales ophiolite complex. The explosive eruption of 15 June 1991 was one of the largest eruptions in the world in the 20th century, but relatively small in the eruption history of the volcano. The 500-year repose before the 1991 eruption is comparatively short for the history of Pinatubo. Prehistoric eruption products are similar to those of the 1991 eruption and record evidence of repeated injections of mafic magmas into a gas-charged dacitic magma chamber (Pallister et al. 1996).

The explosive eruption on 15 June 1991 followed a few weeks of increasing discharge of volcanic gases and seismic activity. Small explosions on 2 April were the

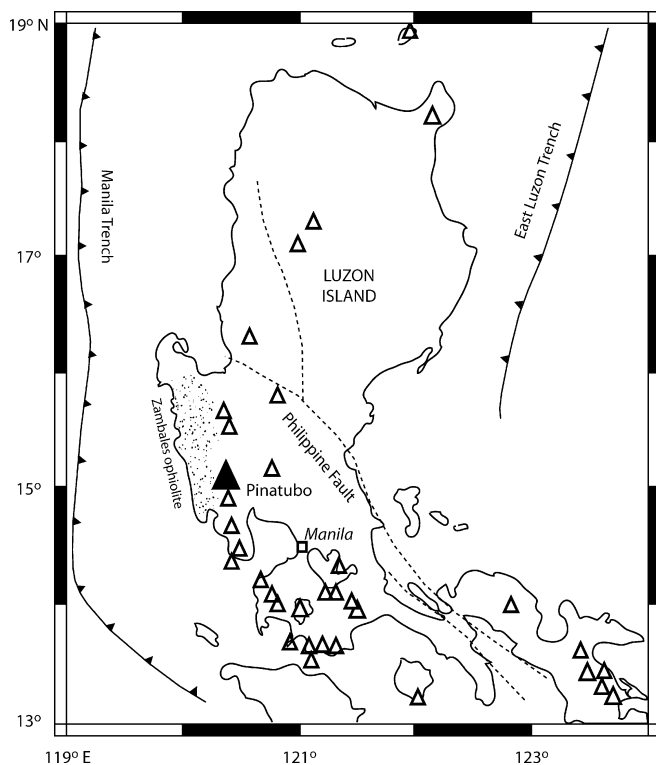


Fig. 1 Regional map of northern Luzon island, Philippines, indicating the active volcanic arc and tectonic features. The Luzon arc, including Pinatubo, is the result of the eastward subduction of oceanic crust along the Manila trench

first sign of the 1991 activity, which were followed by the formation of new fumaroles and degassing of increasing amounts of SO₂, up to 5 kton/day. A dome was sighted on 7 June and was accompanied by intense discharge of ash and SO₂, 10 kton/day on 10 June. The first large eruptions, with eruption columns exceeding 24 km, were recorded on 12 June and produced pyroclastic flows and surges. The eruption products were mostly andesitic in composition, but became increasingly dacitic during the next several days. The climactic eruption on 15 June produced dacitic tephra, 2–10 km³ dense rock equivalent, covering the area of about 2,000 km² (Newhall and Punongbayan 1996).

Various aspects of the eruption history and products and long-term effects on the environment have been documented in the book “Fire and mud: eruptions and lahars of Mount Pinatubo, Philippines”, published jointly by the Philippine Institute of Volcanology and Seismology and the US Geological Survey (Newhall and Punongbayan 1996), and available online at <http://pubs.usgs.gov/pinatubo/>.

Eruption products

The main product of the 1991 eruptions was dacite pumice, which accounts for about 95% of the erupted material. It was very rich in sulfur, mostly in the form of anhydrite, although rare sulfides are present. Primary anhydrite is very uncommon in volcanic rocks and has been reported in only a few locations, such as Mount Lamington in Papua New Guinea (Arculus et al. 1983), El Chichón in Mexico (Luhr et al. 1984), and Lascar in Chile (Matthews et al. 1994). High oxygen fugacities of the magmas are required to stabilize anhydrite (Carroll and Rutherford 1987).

Small volumes of hybrid andesite were erupted as lava during the dome-building phase (7–12 June) and as scoria in the pyroclastic flows and surges that preceded the paroxysmal activity (12–15 June). The hybrid andesite contained quenched fragments of basaltic magma, which are the focus of this study. The andesite is regarded as a mixing product of dacitic and basaltic magmas based on the zoning patterns of plagioclase, disequilibrium textures of minerals (e.g., cummingtonite and anhydrite), the presence of mineral overgrowths (e.g., hornblende rims on olivine, magnetite rims on ilmenite, clinopyroxene rims on quartz), and the variability of matrix glass compositions (Hattori and Sato 1996; Pallister et al. 1996). Phenocrysts of quartz, cummingtonite, plagioclase, and anhydrite were derived from dacite, whereas olivine, clinopyroxene, and hornblende originate from basaltic magma.

Basalt is only observed as fragments of variable size in andesitic dome lava and scoria. The abundance of these fragments is very low. The basaltic fragments lack chilled margins, but textural evidence, such as cusped and interfingering contacts, indicates that the basalt was

partially molten when it was included in the andesite (Bernard et al. 1996; Pallister et al. 1996). The volumes of dome lava and scoria were very small compared with the dacitic eruption products and, therefore, the existence of basaltic magma was mostly destroyed by the following 15 June climatic eruption.

Samples and analytical methods

Five samples of the 1991 eruption that contained basaltic fragments were used for this study (Table 1). They included a large (>1.5 m) basaltic fragment in dome-forming andesite (7–14 June dome) that was ejected during the eruption on 15 June. Other samples were obtained from andesitic scoria of 12 June pyroclastic deposits. The scoria contained small (<1 cm) basaltic fragments and andesitic fragments that enclosed small mafic inclusions (several millimeters in diameter). Both mafic fragments and mafic inclusions were used in this study.

The chemical compositions of minerals, melt inclusions and groundmass glass were determined by electron microprobe at the Ottawa-Carlton Geoscience Centre (Camebax MBX equipped with 4 WDS). Operating conditions were as follows: accelerating voltage 15 kV, beam current 20 nA, spot size 100 μm^2 . Raw data were corrected using a ZAF algorithm. Natural minerals were used as standards and VG2 basaltic glass was used as a secondary standard to monitor accuracy between runs. Additional data on chromites were acquired by SEM at GVC in Gothenburg, Sweden. The system is equipped with a LINK EDS system. Operating conditions were as follows: accelerating voltage 25 kV, beam current 2 nA, spot size <10 μm^2 . No systematic inter-laboratory differences were observed. Counting times vary for different elements as to reach better than 2% precision on major elements, better than 5% on minor elements (Cl and Ti in glass; Ca in olivine; Ti in Cr-spinel; K and Ti in hornblende) and better than 10% on trace elements (P, Mn, and S in glass; Ni and Mn in olivine; Ni, Mn, Si, and Ca in Cr-spinel; Mn in hornblende). Typical run times are 10–20 s for major elements, and 60–100 s for minor elements. Barite was used as the standard for S. The sulfur peak position was determined on several inclusions (see below); as they showed little variation the average position was used as peak position for the sulfur analysis of all other inclusions. The detection limit was ~80 ppm. Repeat analyses of VG2 gave $1,380 \pm 60$ ppm, which is within error of the average value of 1,350 ppm reported in the literature (De Hoog 2001).

Table 1 Sample description

Sample number	Description
P11	Large basaltic fragment (>1.5 m) in dome-forming andesite (7–14 June dome)
P-sco-1 ^a	Andesitic scoria containing small basaltic fragments (<5 mm) from pyroclastic flow probably emplaced on 12 June 1991
P-bas-2	Andesite scoria containing small basaltic fragments (<5 mm) from tephra discharged on 12 June 1991
P-bas-1 #1, #2	Small basaltic fragments (~1 cm) from pyroclastic flow probably emplaced on 12 June 1991
P2–28–92–2	Small basaltic fragment (~2 cm) from pyroclastic flow probably emplaced on 12 June 1991

^aThe scoria contains andesitic fragments and these fragments contain small basaltic inclusions of several mm in diameter. These basaltic inclusions in andesite fragments were also used for this study

The proportion of sulfur species, SO_4^{2-} and S^{2-} , in glasses was determined using the peak position of S-K $_{\alpha}$ (Carroll and Rutherford 1988) by step-wise counting of the sulfur signal by 50 steps of $4 \times 10^{-5} \sin\theta$ for 10 s/step and applying a Gaussian fit over the wavelength scan. Because of the low signal intensity and the possible oxidation of S^{2-} after prolonged exposure to the electron beam (Métrich and Clochiatti 1996) the analysis was limited to glasses with more than 500 ppm S. The precision of the method, based on three repeats on one S-rich inclusion, is $3 \times 10^{-5} \sin\theta$ (1 σ error), which translates to a deviation of less than 10% of measured $\text{SO}_4^{2-}/[\text{SO}_4^{2-} + \text{S}^{2-}]$ compared with the real value.

The bulk-rock composition of the basalt could only be determined on the large basalt fragment (sample P11). Its major element composition was analyzed by XRF on a fused glass disk. The sulfur content was determined with a Leco Simultaneous Carbon/Sulfur Determinator. LOI was determined after igniting samples for over 1 h at 1,050 °C.

Results

Petrography and mineral chemistry

Detailed descriptions of petrography and mineral chemistry of the basalt appear in Pallister et al. (1996) and Bernard et al. (1996). The most important features are repeated below, together with our own observations.

The mineralogy and texture of mafic fragments and inclusions are essentially identical, independent of their size. They are classified as olivine–hornblende basalt containing 30–35 vol% hornblende, ~5 vol% olivine, 10–20 vol% clinopyroxene, 10–15 vol% plagioclase, <1 vol% Fe–Ti oxides and chromite, and trace amounts of sulfides, the remainder being groundmass glass. In addition, several samples contain xenocrystic amphibole and plagioclase phenocrysts that were derived from the dacite (Bernard et al. 1996; Hattori and Sato 1996; Pallister et al. 1996). Xenocrystic amphibole shows reaction rims, and plagioclase contains dusty cores, and corroded rims. Groundmass glass is vesicular, and contains abundant plagioclase microlites. Several small mafic inclusions (several millimeter in diameter) in andesite fragments of scoria lack xenocrystic minerals and contain less clinopyroxene.

Olivine is entirely surrounded by hornblende overgrowth and hornblende microphenocrysts. It shows a narrow compositional range, Fo_{86-88} (Table 2) and no zoning. It contains abundant 5–25- μm -sized euhedral inclusions of Cr-spinel (Fig. 2), which show a compositional range of $\text{Cr}/[\text{Cr} + \text{Al}] = 0.46-0.72$ (Table 2) with most values clustering around 0.64. The chromite inclusions give a clue about the origin of hosting olivine. The texture of olivine clearly indicates that it was unstable in the final assemblage, which prompted the proposal that it is a xenocryst originated from underlying Zambales ophiolitic complex. We discard this possibility. First, high contents of Fe^{3+} and Ti in Pinatubo chromite are distinctly different from those in Zambales ophiolite complex (Fig. 3), as pointed out by Pallister et al. (1996). Second, olivine in our samples contains significant CaO (0.1 to 0.3 wt%), which is indicative of crystallization at low pressures, and, again, is not

Table 2 Chemical compositions of selected Cr-spinel–olivine pairs, calculated oxidation states and equilibration temperatures. *n.a.* not analyzed

Sample	P11	P11	P-bas-1#1	P-bas-1#1	P-bas-1#2	AVG (<i>n</i> = 15)	SD
Cr-spinel							
SiO ₂ ^a	0.15	0.11	0.60	<i>n.a.</i>	<i>n.a.</i>	0.22	± 0.16
TiO ₂	0.84	0.72	1.05	1.06	0.80	0.92	± 0.10
Al ₂ O ₃	15.05	13.98	16.06	15.28	20.19	15.61	± 1.48
Cr ₂ O ₃	40.78	42.97	35.49	37.98	36.28	39.04	± 2.06
Fe ₂ O ₃	11.58	12.72	14.68	15.06	12.93	13.65	± 1.02
FeO	18.93	16.81	19.16	19.74	17.82	18.78	± 1.26
MnO	0.25	0.20	0.20	0.50	0.46	0.33	± 0.12
NiO	0.11	0.19	0.11	<i>n.a.</i>	<i>n.a.</i>	0.08	± 0.07
MgO	9.90	11.33	10.28	9.57	11.36	10.26	± 0.93
CaO	0.02	0.02	0.16	0.09	0.08	0.06	± 0.04
Total	97.61	99.05	97.79	99.28	99.93	98.95	± 1.43
X _{Cr} ^b	0.65	0.67	0.60	0.63	0.55	0.63	± 0.03
X _{Mg}	0.48	0.55	0.49	0.46	0.53	0.49	± 0.04
Olivine							
SiO ₂ ^a	40.09	38.29	40.06	40.55	40.79	40.16	± 0.67
FeO	12.51	11.57	12.96	13.22	12.05	12.38	± 0.50
MnO	0.21	0.20	0.23	0.21	0.20	0.20	± 0.03
NiO	0.18	0.24	0.11	0.13	0.30	0.20	± 0.05
MgO	46.67	47.65	46.23	47.17	48.10	47.42	± 0.75
CaO	0.18	0.16	0.18	0.21	0.13	0.18	± 0.02
Total	99.84	98.11	99.77	101.49	101.57	100.54	± 1.19
Fo	86.9	88.0	86.4	86.4	87.7	87.2	± 0.5
T _{closure} (°C) ^c	833	930	861	839	829	852	± 62
ΔNNO	1.17	1.32	1.55	1.57	1.42	1.47	± 0.14

^aAll oxides in wt% by electron microprobe or SEM; Fe₂O₃ and FeO calculated from FeO* assuming ideal spinel stoichiometry

^bX_{Cr} = atomic ratios of Cr/(Cr + Al), X_{Mg} = atomic ratios of Mg/(Mg + Fe²⁺)

^cOxidation states and closure temperatures (temperature of last equilibration) calculated following the model by Ballhaus et al. (1990, 1991), assuming *P* = 0.22 GPa and using the closure temperature for calculation of oxidation states

consistent with the derivation of olivine from the ophiolite complex. Furthermore, the narrow range of olivine compositions and the fact that Mg/Fe ratios of olivine (Fo_{86±1}) are in equilibrium with that of the bulk rock suggest that olivine grew as phenocrysts in the hosting basalt, and it is not likely incorporated from old eruption products.

Amphibole occurs as overgrowths on olivine, small (< 100 μm) euhedral, mostly elongated microphenocrysts, and large (> 5 mm) elongated xenocrystic crystals with reaction rims. The xenocrystic crystals are (ferri-) magnesio-hornblende, whereas the overgrowths and small crystals are magnesio-hastingsite (Table 3), following the classification of Leake et al. (1997). Diopsidic clinopyroxene occurs as small euhedral crystals often associated with amphibole. Plagioclase occurs as small euhedral phenocrysts, microlites in the groundmass, and, occasionally, as large xenocrystic crystals. Other minor minerals are magnetite, ilmenite, plagioclase, quartz, and sulfides. Sulfide phases are globular nickel-bearing pyrrhotite and irregularly shaped copper-rich sulfides. They are common in amphibole phenocrysts, but are very rare in olivine, where they usually are in contact with or very close to amphibole. Copper-rich sulfides were only observed in the groundmass.

Melt inclusions have not been identified in any of the olivine grains throughout the course of this study. Exceptions are a few highly evolved inclusions connected to the olivine surface by cracks. Therefore, we conclude that rare melt inclusions in olivine are of secondary origin, i.e., late-stage melts intruded into the mineral through cracks. In contrast, melt inclusions are

common in small euhedral amphiboles. Rounded or irregular-shaped glassy inclusions of 10 to 50 μm in size commonly occupy a significant portion of the core of the mineral (Fig. 2B). They are primary inclusions using the criteria defined by Roedder (1984). The inclusions are free of vapor bubbles and daughter minerals, but may contain contraction bubbles along the inclusion walls (< 2% of inclusion volume), which result from volume contraction of the inclusions during cooling. Melt inclusions occur sporadically in magnetite, ilmenite, or plagioclase, in which they occasionally contain daughter minerals.

Composition of melt inclusions and matrix glass

We limit our results and discussion to melt inclusions in amphibole because they are the most abundant, have the least-evolved compositions, and do not contain daughter minerals, and also to reduce the possible effects of post-entrapment crystallization.

The melt inclusions show a continuous compositional range from 62.7 to 74 wt% SiO₂ (Table 3, Fig. 4) and exhibit more or less linear arrays in major-element space, usually trending towards groundmass glass compositions. Al₂O₃ contents decrease from 19.5 to 14 wt% with increasing SiO₂, whereas CaO contents decrease from 5.5 to 1.5 wt%. MgO contents are very low (mostly < 1 wt%) and more or less constant. K₂O contents are relatively high (mostly between 2.5 and 4 wt%).

Compared to bulk-rock compositions the melt inclusions show significantly higher SiO₂, K₂O, and Na₂O, lower CaO and MgO, and a wider range of Al₂O₃

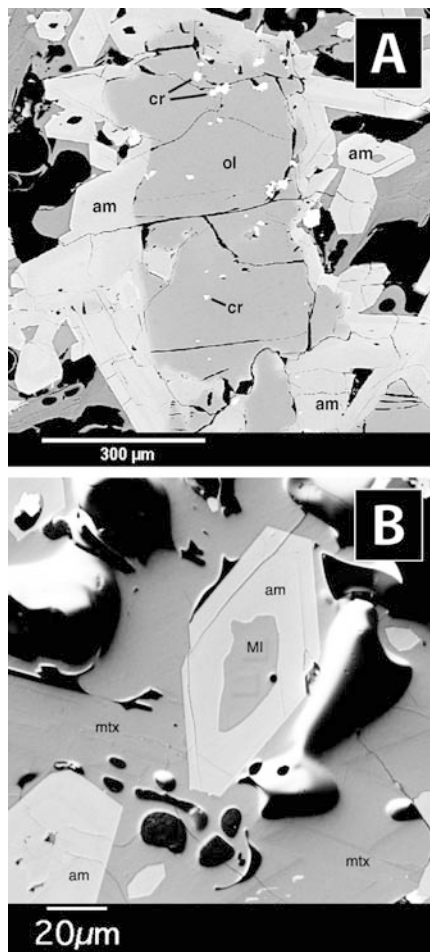


Fig. 2 **A** Back-scattered electron image of Cr-spinel inclusions in olivine in sample P11 (*ol* olivine, *cr* Cr-spinel, *am* amphibole). Note the amphibole overgrowth on the olivine. Olivine–Cr-spinel pairs indicate an oxidation state of the basalt of about $\text{NNO} + 1.4$ before the mixing event (see text). **B** Back-scattered electron image of a melt inclusion in amphibole in sample P-bas1#1 (*am* amphibole, *MI* melt inclusion, *mtx* groundmass consisting of glass and plagioclase microlites). A small contraction bubble is visible along the inclusion wall. The faint squares in the melt inclusion show the location of the electron beam during analysis. The small euhedral amphibole crystallized during the mixing of basaltic and dacitic magmas, and this mixing is recorded by the compositional variation of the melt inclusions

contents. In addition, compositional variations of the melt inclusions can be quite different from those of bulk-rock composition data. For example, the Al_2O_3 content of the bulk rock increases with increasing SiO_2 content, whereas it decreases in melt inclusions (Fig. 4A). A similar trend is observed for NaO, whereas CaO and FeO follow bulk-rock trends.

Sulfur contents of melt inclusions range from 125 to more than 1,700 ppm; the highest values are in the inclusions with lowest SiO_2 (Fig. 4B). The amount of sulfur present as SO_4^{2-} is $85 \pm 10\%$, based on the S-K α peak shift of five inclusions. Chlorine contents of melt inclusions are scattered, ranging mostly from 1,900 to 2,600 ppm, and show no clear correlation with any other

chemical parameters. The amount of $\text{H}_2\text{O} + \text{CO}_2$ is estimated to be ca. 2 ± 1 wt% based on the sums of oxides, Cl, and S.

The groundmass of basaltic fragments consists of abundant microlites and rhyolitic glass (69–75 wt% SiO_2), which is compositionally similar to the most evolved melt inclusions. The sulfur content of groundmass glass ranges from less than 90 to 260 ppm with high values from relatively large basaltic fragments. These values are much lower than those of most melt inclusions. The amount of sulfur is too low to obtain reliable estimates of the proportion of sulfate sulfur. The average Cl content of groundmass glass is 1,700 ppm, which is about 500 ppm lower than that of melt inclusions.

Discussion

Mixing trends defined by melt inclusion data

The major element contents of melt inclusions in the basaltic fragments show linear variations between andesitic (~ 62 wt% SiO_2) and rhyolitic (~ 75 wt% SiO_2) compositions (Fig. 4). Considering that the andesitic rocks formed by mixing between dacitic and basaltic magmas, the two end members likely correspond to the melt phases in the two magmas: rhyolitic melt inclusions represent the melt phase of the dacitic magma and andesitic melt inclusions represent the melt phase of the basaltic magma. Indeed, the melt inclusions with a rhyolitic composition are very similar to groundmass glass and melt inclusions of the dacitic eruption products reported by Luhr and Melson (1996) and Pallister et al. (1996). The end-member composition of the andesitic melt is unknown because groundmass glass in the basaltic samples has been changed by the formation of microlites, which crystallized in response to rapid cooling of the magma during the mixing with the felsic magma. Therefore, we estimated the composition of melt in the basaltic magma prior to mixing with a simple mass-balance model using the modal abundances of phenocrysts, their mineral chemistry, and the bulk-rock composition of the basalt. The result shows that the melt had an andesitic composition similar to the least evolved melt inclusions (Table 4). Therefore, we conclude that the least evolved melt inclusions are representative of, or at least close to, the melt phase of the basalt at the onset of mixing. Hence, the melt inclusions in amphiboles represent the entire range of compositions of melt during the mixing between basaltic and dacitic magma.

We envisage the following sequence of events. Before intrusion, the basaltic magma had crystallized olivine and clinopyroxene, and its melt component had evolved to an andesitic composition. When the basaltic magma was injected into the dacitic magma, andesitic melt and rhyolitic melt components of the two magmas started mixing. The mixing resulted in the crystallization of

Fig. 3 Compositional variation of Cr-spinel inclusions (*gray diamonds*) in olivine from basaltic fragments in a ternary diagram. The data are compared with spinel from dacite (two fields), andesite and basalt (Bernard et al. 1996) and the Zambales ophiolite complex (Yumul 1992). Note the distinctly different compositions of Cr-spinel from the Zambales ophiolite, which partially underlies Mount Pinatubo (Fig. 1)

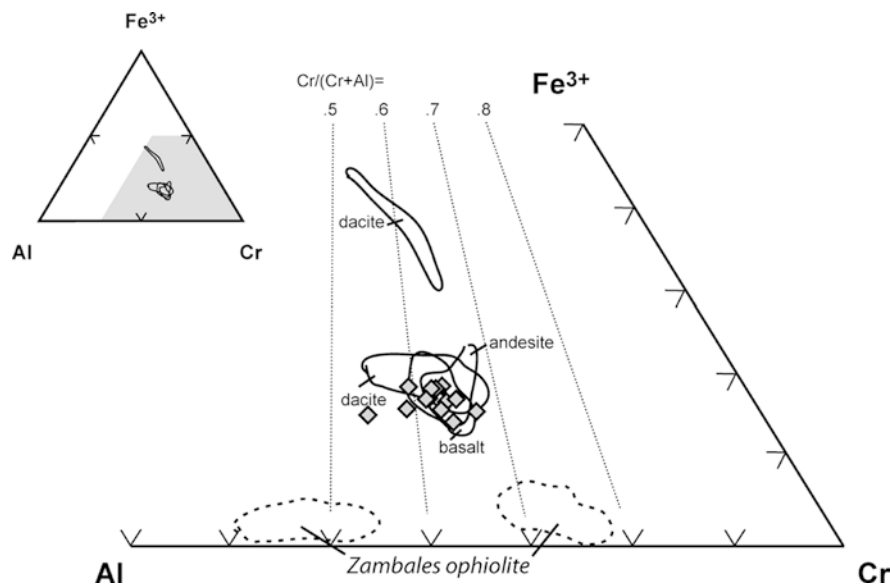


Table 3 Representative chemical compositions of melt inclusions and amphibole in basaltic fragments, and bulk-rock composition

Sample/analysis	P-bas-1 #1-14	P-sco-1 10	P-bas-1 #1-01	P2-28-92-2-2	P-sco-1 13	P-sco-1 13h	P11
Type	MI ^a	MI	MI	MI	MI	am ^b	Bulk rock ^c
SiO ₂	62.63	65.66	61.19	68.88	74.14	41.06	50.76
TiO ₂	0.19	0.24	0.21	0.23	0.31	1.72	0.89
Al ₂ O ₃	19.56	18.47	18.46	16.76	14.18	12.72	14.35
Fe ₂ O ₃ ^d						8.30	
FeO	3.72	2.86	3.67	2.32	2.71	7.39	8.25
MnO	0.24	0.16	0.24	0.15	0.10	0.22	0.16
MgO	0.66	0.59	0.70	0.60	0.51	12.10	8.96
CaO	4.81	3.73	5.19	2.02	1.50	11.33	10.08
Na ₂ O	4.63	4.47	4.32	4.39	2.73	2.19	2.96
K ₂ O	2.98	3.31	2.89	4.60	3.49	0.58	1.56
P ₂ O ₅	0.58	0.52	0.54	0.06	0.33		0.32
Total ^e	97.25	98.18	97.42	99.04	98.44	97.62	99.61
LOI							0.40
Cl ^f	2,250	2,120	2,250	2,090	2,230		
S	1,710	910	1,250	260	370		400
FeO/FeO ^T						0.50	
Mg#						0.74	
#Si						6.07	
#(Na + K) _A						0.53	

^aMelt inclusions in amphibole by electron probe

^bComposition of amphibole typical for those hosting the melt inclusions by electron probe; Mg# = Mg/[Mg + Fe²⁺]; #Si = number of Si atoms in the formula based on 23 O; #(Na + K)_A = number of Na and K atoms in the A-site following the formula by Leake et al. (1997)

^cComposition of bulk rock by XRF

^dAll Fe as FeO except for amphibole mineral, where Fe₂O₃ and FeO are calculated based on stoichiometry

^eAll oxides for melt inclusions are recalculated to 100 wt% volatile free; totals are totals of analysis before normalization

^fS and Cl in ppm

amphibole (magnesio hastingsite) as microlites and overgrowths on and replacement of olivine crystals in the basaltic magma. Rapid amphibole growth resulted in the formation of abundant melt inclusions. The mixing formed the dome-forming andesite and scoria in pyroclastic flow deposits preceding the climatic eruption of 15 June. The mixing was recorded in the compositional variation of the melt inclusions reported in this study.

Oxidation state of the basaltic magma

Sulfur in silicate melt occurs mostly as S²⁻ and SO₄²⁻, the relative abundance of which varies with the oxidation state of the melt (Carroll and Rutherford 1988). Small amounts of SO₃²⁻ (< 15%) may also be present (Métrich et al. 2003). The melt inclusions from this study contain ~85% of sulfur as sulfate. The oxidation state is

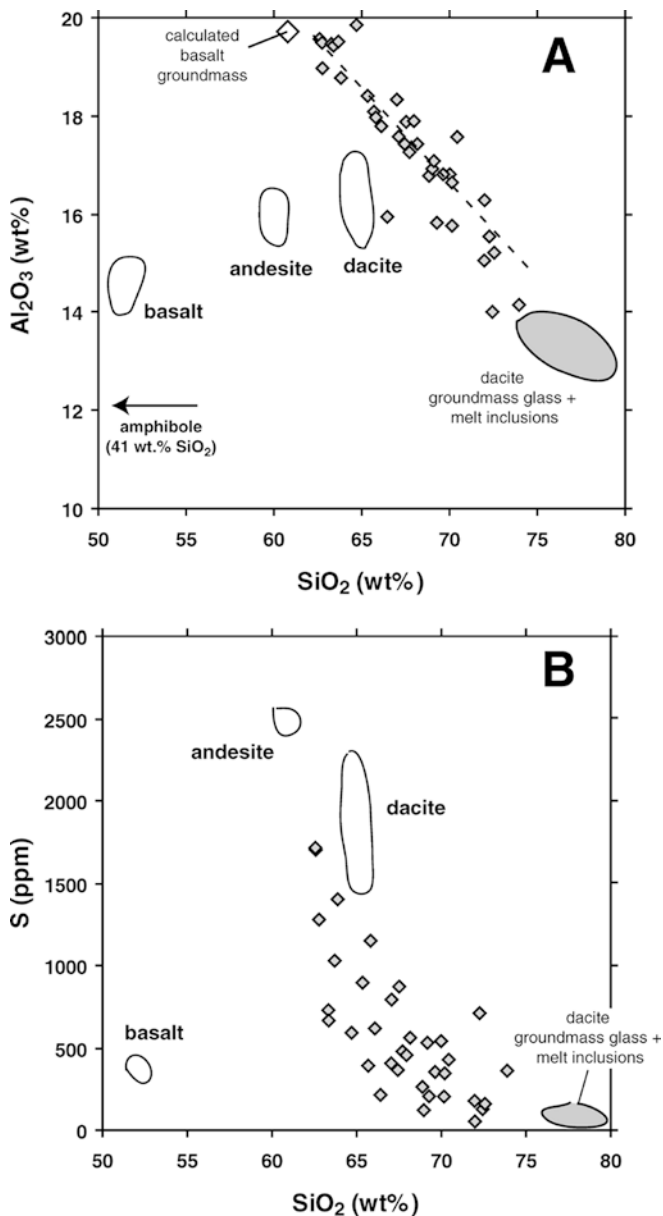


Fig. 4 A Al_2O_3 – SiO_2 and B S– SiO_2 variation diagrams. *White fields* indicate bulk rock compositions of dacite, andesite and basalt (Bernard et al. 1996; Pallister et al. 1996; this study). The *gray field* corresponds to the compositions of groundmass glass and melt inclusions in the dacitic eruption products. The compositions of melt inclusions in basaltic fragments are indicated by *gray diamonds*. The groundmass composition of the basalt magma, shown as an *open diamond* in A, was calculated from the composition of bulk rock and phenocrysts (see text). The composition of amphibole that hosts the melt inclusions is shown with an *arrow* in A. If significant post-entrapment crystallization would have taken place in the melt inclusions, the compositions would have fit an amphibole control line. Note that in A the melt inclusions compositions define a linear mixing line between the rhyolitic groundmass glass in dacitic magma and andesitic groundmass glass in basalt magma. Similar trends are observed for other major elements

calculated to be around $\text{NNO}+1.3$ (± 0.5) using the relationship between $f\text{O}_2$ and sulfur speciation in magma by Wallace and Carmichael (1992). The value

Table 4 Representative chemical compositions of phenocrysts, bulk rock and calculated groundmass of basalt magma. *am* hornblende; *ol* olivine; *cpx* clinopyroxene; *pl* plagioclase; *ox* Fe–Ti oxide; *bulk* bulk-rock composition (sample P11); *mtx* calculated groundmass composition based on compositions and modal amounts of phenocrysts and bulk rock; all compositions are normalized to 100 wt% volatile-free

	am	ol	cpx	pl	ox	bulk	mtx
vol%	32.5	5	15	12.5	0.5	100	34.5
SiO_2	42.9	40.9	51.7	55.7	-	51.7	61.0
TiO_2	2.0	-	0.5	-	7.6	0.9	0.4
Al_2O_3	12.7	-	3.9	27.3	3.0	14.6	18.8
FeO^*	13.9	12.0	5.5	1.0	86.4	8.7	6.5
MnO	0.2	0.2	0.1	-	0.5	0.2	0.2
MgO	13.3	46.7	15.0	-	2.5	9.1	0.6
CaO	12.0	0.2	22.9	10.2	0.1	10.3	4.8
Na_2O	2.4	-	0.3	5.4	-	3.0	4.2
K_2O	0.6	-	0.0	0.3	-	1.5	3.5

represents the oxidation state of the mafic magma at the onset of mixing because it was obtained from the least-evolved melt inclusions.

The oxidation state of the mafic magma before the mixing event is obtained using the composition of co-existing olivine and spinel (Ballhaus et al. 1990, 1991). We selected chromite grains in the cores of olivine for olivine–spinel geobarometry (Fig. 2A). Ferric iron in spinel was calculated assuming stoichiometry, following the recommendation by Ballhaus et al. (1991). The chromite–olivine pairs yield a mean oxidation state of $\text{NNO}+1.47$ (Table 2; Fig. 5), which is similar to the oxidation state obtained from the sulfur speciation of melt inclusions. Both chromite and olivine cores were not in contact with the felsic melt during the mixing between felsic and mafic magmas; thus, the composition of the pairs provides the condition of mafic magma before intrusion and mixing. Although not explicitly included in the calibration, the oxygen barometer requires the presence of orthopyroxene as a buffer of SiO_2 . Orthopyroxene is not present in Pinatubo basalt, but the barometer is still applicable to the samples provided that the calculated $f\text{O}_2$ is corrected for the undersaturation of orthopyroxene. As the correction for mantle-derived melts rarely exceeds -0.2 log units, which is less than the error in the calibration (0.4 log units; Ballhaus et al. 1991), no correction was applied to our results.

Equilibrium temperatures from chromite–olivine pairs (algorithm of Fe–Mg exchange between olivine and spinel; Ballhaus et al. 1991) range from 820 to 930 °C (Table 2; Fig. 5), which is higher than the temperature of the dacite magma (~ 760 °C; Scaillet and Evans 1999), but considerably lower than estimates for the basaltic magma using other methods: 960–1,140 °C (Hattori and Sato 1996), $\sim 1,150$ °C (Rutherford and Hammer 2001), and $\sim 1,200$ °C (Pallister et al. 1996). The low temperatures obtained from the chromite–olivine pairs can be explained by a minor degree of cation exchange between chromite and host olivine. The subsolidus reaction strongly affects temperature

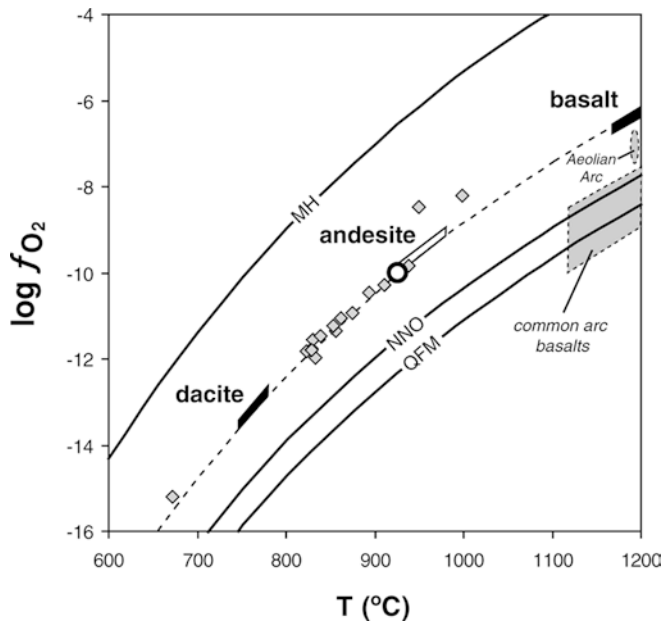


Fig. 5 Estimated $\log f_{\text{O}_2}$ and temperatures of Pinatubo basaltic magma (solid field) based on f_{O_2} values obtained from Cr-spinel-olivine barometry (this study) and temperature estimates from Pallister et al. (1996). Calculated f_{O_2} -temperature values from individual olivine-spinel pairs are shown in gray diamonds, which plot at lower temperatures due to rapid cooling of basaltic fragments. Note, however, that f_{O_2} estimates are insensitive to temperature estimates (Ballhaus et al. 1991). The open circle shows the temperature of basaltic fragment using sulfide-olivine geothermometry assuming NNO+1.5. For comparison, the fields for Pinatubo dacite (Scaillet and Evans 1999), andesite (Pallister et al. 1996), Aeolian arc (Métrich and Clocchiatti 1996) and common arc basalt (e.g. Carroll and Webster 1994) are shown. MH, NNO and QFM indicate magnetite-hematite, nickel-nickel oxide and quartz-magnetite-fayalite oxygen buffers, respectively. The dashed line is NNO+1.5.

estimates, but does not significantly affect estimates of oxidation conditions (Ballhaus et al. 1991). As the basalt was not erupted immediately, but was entrained in hybrid andesite first, which had a temperature of 930–960 °C (Pallister et al. 1996), the low equilibration temperatures are not surprising.

The oxidation state of the mafic magmas is comparable to the most recent estimate of the oxidation state of the dacite melt (NNO+1.5 to +1.7; Scaillet and Evans 1999)¹. Furthermore, the high oxidation condition is similar to that of the dome-forming andesite based on the Fe-Ti-oxide barometry (Hattori 1996), but the data were interpreted to show fast re-equilibration of Fe-Ti oxides in the dacitic magma. Our new results suggest that the mafic magma already had a high oxi-

dation state prior to injection into the felsic magma. These high ΔNNO values are among the highest values reported from arc basalts yet; at least equal to values reported from Lascar (Matthews et al. 1999) and considerably higher than oxidation states of primitive melts from the Aeolian Arc ($\leq \text{NNO} + 1$; Métrich and Clocchiatti 1996).

Mafic fragments at Mount Pinatubo contain sulfide globules, which were interpreted as evidence of a reduced condition of the mafic magma (Matthews et al. 1992; Hattori 1993, 1996; Kress 1997). Our proposed interpretation, a high oxidation state of the mafic melt, seems counterintuitive, as the formation of sulfide requires S^{2-} in the melt. Sulfur in silicate melt occurs as SO_4^{2-} and S^{2-} under a wide range of oxidation conditions, and sulfide formation takes place once the silicate melt is saturated with S^{2-} , even though the melt contains SO_4^{2-} as the predominant sulfur species. Recent experimental work by Scaillet and Evans (1999) confirms that sulfide can form in silicate melt at relatively high oxidation states (up to NNO+1.4).

In order to confirm the unexpectedly high oxidation state of the basalt, we considered various other oxygen barometers. Poustovetov and Roeder (2000) calibrated an oxygen barometer based on the composition of chromite in equilibrium with silicate melt. This oxybarometer is highly dependent on the Cr content of melt, which is impossible to estimate in our samples because of the lack of primitive inclusions in olivine. Similar reasons did not permit the use of vanadium-based crystal-melt oxybarometers (e.g., Canil 1995). Brenan and Caciagli (2000) calibrated a Fe-Ni sulfide-olivine barometer. Sulfides are very scarce in olivine in our samples and always occur in contact with or near hornblende overgrowth. The compositions of two sulfide grains (our unpublished data) near hornblende yielded oxygen fugacities of $\log f_{\text{O}_2} = 10^{-9.8}$ and 10^{-10} . Conversion of this value relative to oxygen buffers is strongly temperature dependent. The use of the temperature of olivine growth ($\sim 1,200$ °C) results in an oxidation state of NNO-2.2, which is unrealistically low. Therefore, we suspect equilibration of olivine-sulfide Fe-Ni exchange at lower temperatures. If we assume an oxidation state of NNO+1.5 for the basalt magma, the closure temperature of Fe-Ni exchange is calculated to be ~ 930 °C (Fig. 5), which is close to the estimated temperature of the hybrid andesite based on Fe-Ti oxide thermometry (903–960 °C; Pallister et al. 1996). We suggest that temperatures of the small basalt fragments quickly re-equilibrated to that of the andesite host.

Sulfur content of the basaltic magma

The sulfur content in the least-evolved melt inclusions, $\sim 1,700$ ppm, is high compared with sulfur contents in mid-oceanic ridge basalt (MORB; Wallace and Carmichael 1992; Nilsson and Peach 1993), especially

¹Earlier estimates of the oxidation state of the dacitic magma (NNO+2 to +3) were made using Fe-Ti oxides in the eruption products (Matthews et al. 1992; Hattori 1993; Pallister et al. 1996). Recent experimental work (Evans and Scaillet 1997) showed that Fe-Ti-oxide oxygen barometry used by previous workers overestimates oxidation states outside its calibration range. Re-calibrated values indicate an oxidation state between NNO+1.5 to +1.7.

considering the andesitic composition of the most sulfur-rich melt inclusions. It has been shown experimentally and empirically that sulfur solubility is high in oxidized melts (e.g., Luhr et al. 1990; Métrich and Clocchiatti 1996), and our results are in line with those studies.

The initial sulfur content of the basaltic magma is unknown, but is likely to have been high. Even if we assume that the sulfur dissolved in the melt is concentrated by crystallization of olivine and clinopyroxene, and ignore the presence of sulfides, the sulfur content of the primary melt must have been at least ~1,200 ppm. The initial sulfur content was likely to be higher because sulfides were present (which total about 300 ppm S based on the difference between bulk-rock and groundmass sulfur contents), the melt was sulfur-saturated and may have lost sulfur by segregation of immiscible sulfide liquid, and because degassing likely started during the ascent of the basaltic magma from mantle depths. In any case, the basalt magma had a much higher dissolved sulfur content than the dacite.

Source of SO₂ discharged to the atmosphere

We demonstrated above that the basaltic magma that intruded the dacite magma chamber was S-rich and relatively oxidized, and that the oxidation state of the basaltic magma was comparable to that of the dacitic magma. The findings are not consistent with various models proposed by previous researchers, that suggested that sulfur was released during mixing between S-rich, reduced basalt and oxidized dacite (Matthews et al. 1992; Hattori 1993; Kress 1997). Our data show no significant change in oxidation state during mixing. Therefore, the intruded basaltic magma cannot have been the (immediate) source of sulfur during the eruption.

Mafic magmas discharge sulfur as SO₂ during ascent in response to temperature decrease and solidification of the magmas. SO₂ may be discharged together with a CO₂-H₂O fluid, the solubility of which decreases sharply with decreasing pressure (Holloway and Blank 1994). High CO₂ concentrations were reported in glass inclusions of the dacite magma, and were thought to be derived from underplated basalt (Wallace and Gerlach 1994). As documented by late sulfides with high As and Sb in the groundmass glass of the dacite (Hattori 1993, 1996), SO₂ escaping from mafic magma was first fixed in the overlying dacite magma as sulfides and anhydrite, whereas additional SO₂ was incorporated into aqueous fluids in the magma chamber. Anhydrite crystallization continued after fluid saturation as indicated by growth textures of anhydrite (Jakubowski et al. 2002). Abundant aqueous fluid inclusions in phenocrysts (Hattori 1996) point to the presence of immiscible aqueous fluids in the dacite magma chamber (Westrich and Gerlach 1992; Gerlach et al. 1996). Sulfur dissolved in the fluids

was readily available for discharge to the atmosphere during eruption.

Injection of mafic magmas is considered to be a replenishing process of crustal silicic magma chambers (Sparks et al. 1977). The ascent and solidification of mafic magmas result in the transfer of volatiles to overlying silicic magma reservoirs. Therefore, accumulation of vapor in silicic magma chamber, as we propose here, is probably common in volcanoes. Wallace (2001) envisaged that vapor degassed from underplated basalts accumulates in overlying silicic magma chambers during long repose periods in-between eruptions, so that silicic magmas are likely to contain 1–6 wt% exsolved gas prior to eruption. Hattori and Keith (2001) suggested that this process is essential for the magmatic-hydrothermal activity leading to the porphyry copper deposits.

The oxidation condition of arc magmas and source mantle

Oxidized felsic igneous rocks are common in island arcs. The distribution of oxidized granitic rocks form arrays parallel to subduction zones (e.g., Ishihara 1981). Oxidized volcanic rocks are also known in arcs. Examples include anhydrite-bearing rocks at El Chichón, Mexico (Luhr et al. 1984), Mt Lamington, Papua New Guinea (Arculus et al. 1983), Nevado del Ruiz, Colombia (Fournelle 1990), Lascar, Chile (Matthews et al. 1994), and Akita-Komagatake, Japan (our unpublished data). The crystallization of anhydrite requires a high oxidation state of these magmas. Proposed causes of the oxidation include assimilation of evaporitic sulfate minerals (Arculus et al. 1983; Luhr et al. 1984), introduction of oxidizing fluids from underlying basalt (e.g., Hattori 1993; Gerlach et al. 1996; McKibben et al. 1996), and preferential loss of reduced gases, such as H₂ (e.g., Carmichael and Ghiorso 1986). Our study shows that the oxidized nature of felsic magmas in shallow crustal reservoirs may reflect parental mafic magmas and, thus, probably reflects the oxidized state of the source mantle.

The oxidation condition of the upper mantle is heterogeneous and varies more than four logarithmic units in *f*O₂. The most oxidized domain is the sub-arc mantle where the oxidation condition is generally above the FMQ buffer because of the addition of oxidized, crustal material and slab-derived melts and fluids (Ballhaus 1993; Parkinson and Arculus 1999; Mungall 2002). The flux of slab-derived materials also enriches the sub-arc mantle in sulfur (De Hoog et al. 2001a, 2001b). Basaltic magma from Pinatubo plots near the high end of the range of oxidation conditions reported from the sub-arc mantle (Ballhaus et al. 1990; Parkinson and Arculus 1999). The highly oxidized state of the sub-arc mantle may be regional beneath the Luzon arc. The Luzon arc is considered to be one of the most fertile arcs in the world, producing numerous

young (<4 Ma) porphyry Cu deposits, including the Santo Tomas and Far Southeast mines. Porphyry Cu deposits contain large quantities of sulfur as Cu sulfides and Fe-sulfides in the deposits themselves and their alteration halos. As the amount of sulfur is too large to be supplied from immediate host rocks, sulfur was likely supplied from mafic magmas (Hattori and Keith 2001). High magmatic oxygen fugacities are favorable for the formation of such deposits (Imai et al. 1993). Considering the distribution of these young porphyry Cu deposits along the arc, it is tempting to suggest that the mantle beneath the Luzon arc is regionally oxidized and capable of producing oxidized, S-rich mafic magmas.

Oxidized basaltic magma is significant as it is capable of transporting higher amounts of sulfur than does more reduced basalt (Carroll and Rutherford 1985). Experimental data suggest that oxidized melt could contain up to 0.5 wt% S (Luhr 1990). It is probably no coincidence that many volcanoes characterized by highly oxidized magmas (e.g., El Chichón, Lascar, Nevado del Ruiz) discharge large quantities of SO₂ (Rampino and Self 1984; Williams et al. 1990; Andres et al. 1991). Oxidized magma contains much sulfur in the form of sulfate; thus, the amount of sulfur removed as immiscible sulfide liquid at lower crustal and upper mantle depths is limited. Furthermore, oxidized magma can effectively scavenge sulfur from sulfides in the source mantle. Thus, oxidized magma can efficiently deliver sulfur from the sub-arc mantle into the shallow crust and to either the atmosphere or to ore-forming fluids.

Conclusions

The mafic magma that intruded the dacitic magma chamber several days before the 1991 Pinatubo eruption was oxidized, ~NNO + 1.5, and S-rich (≥1,700 ppm), as demonstrated by olivine–spinel oxygen barometry and the high SO₄²⁻ content (~85% of S) of the melt inclusions. The oxidation state of the mafic magma was comparable to that of the dacitic magma. The mixing between felsic and mafic magmas was not accompanied by a significant change in the oxidation state of the magma, which dismisses models that invoke mixing as a means of releasing sulfur from the melt during eruption. At Pinatubo, the SO₂ discharged from mafic magma was incorporated in magma and immiscible aqueous fluids in the overlying felsic magma chamber. This sulfur dissolved in the aqueous fluids was likely the source of sulfur that was discharged to the atmosphere during the cataclysmic eruption.

The oxidized state of the felsic magma was likely inherited from mafic magma and ultimately from the sub-arc mantle where the mafic melt originated. Highly oxidized primitive magma, as observed in Pinatubo, would serve as an efficient medium to transfer large

amounts of sulfur from the mantle to the shallow crust. This may explain why many oxidized volcanoes are also known for large discharges of SO₂.

Acknowledgements C. Thornber, T.M. Gerlach, A. Gurenko, and an anonymous journal reviewer are thanked for helpful reviews, which helped to clarify many points in the manuscript. E. Essene and P. Roeder are thanked for stimulating discussions about chromite–olivine oxygen barometry.

References

- Andres RJ, Rose WI, Kyle PR, De Silva S, Francis P, Gardeweg M, Moreno Roa H (1991) Excessive sulfur dioxide emissions from Chilean volcanoes. *J Volcanol Geotherm Res* 46:323–329
- Arculus RJ, Johnson RW, Chappell BW, McKee CO, Sakai H (1983) Ophiolite-contaminated andesites, trachybasalts, and cognate inclusions of Mount Lamington, Papua New Guinea; anhydrite–amphibole-bearing lavas and the 1951 cumulodome. *J Volcanol Geotherm Res* 18:215–247
- Ballhaus C (1993) Redox states of lithospheric and asthenospheric upper mantle. *Contrib Mineral Petrol* 114:331–348
- Ballhaus C, Berry RF, Green DH (1990) Oxygen fugacity controls in the Earth's upper mantle. *Nature* 348:437–440
- Ballhaus C, Berry RF, Green DH (1991) High pressure experimental calibration of the olivine–orthopyroxene–spinel oxygen geobarometer: implications for the oxidation state of the upper mantle. *Contrib Mineral Petrol* 107:27–40
- Bernard A, Knittel U, Weber B, Weis D, Albrecht A, Hattori K, Klein J, Oles D (1996) Petrology and geochemistry of the 1991 eruption products of Mount Pinatubo. In: Newhall CG, Punongbayan RS (eds) *Fire and mud: eruptions and lahars of Mount Pinatubo, Philippines*. PHIVOLCS, Quezon City, Philippines and University of Washington Press, Seattle, pp 767–797
- Brenan JM, Caciagli NC (2000) Fe–Ni exchange between olivine and sulphide liquid: Implications for oxygen barometry in sulphide-saturated magmas. *Geochim Cosmochim Acta* 64:307–320
- Canil D (1995) Vanadium partitioning and the oxidation state of Archaean komatiite magmas. *Nature* 389:842–845
- Carmichael ISE, Ghiorso MS (1986) Oxidation–reduction relations in basic magma: a case for homogeneous equilibria. *Earth Planet Sci Lett* 78:200–210
- Carroll MR, Rutherford MJ (1985) Sulfide and sulfate saturation in hydrous silicate melts. *J Geophys Res* 90C:601–612
- Carroll MR, Rutherford MJ (1987) The stability of igneous anhydrite: experimental results and implications for sulfur behavior in the 1982 El Chichón trachyandesite and other evolved magmas. *J Petrol* 28:781–801
- Carroll MR, Rutherford MJ (1988) Sulfur speciation in hydrous experimental glasses of varying oxidation state: results from measured wavelength shifts of sulfur X-rays. *Am Mineral* 73:845–849
- Carroll MR, Webster JD (1994) Solubilities of sulfur, noble gases, nitrogen, chlorine and fluorine in magmas. In: Carroll MR, Holloway JR (eds) *Volatiles in magmas*. *Rev Mineral* 30:231–280
- De Hoog JCM (2001) Behavior of volatiles in arc volcanism. PhD Thesis, Utrecht University, *Geologica Ultraiectina* 204
- De Hoog JCM, Mason PRD, Van Bergen MJ (2001a) Sulfur and chalcophile elements in subduction zones: constraints from a laser ablation ICP-MS study of melt inclusions from Galunggung Volcano, Indonesia. *Geochim Cosmochim Acta* 65:129–146
- De Hoog JCM, Taylor BE, Van Bergen MJ (2001b) Sulfur isotope systematics of Indonesian arc basalts and implications for the

- sulfur cycle in subduction zones. *Earth Planet Sci Lett* 189:237–252
- Evans BW, Scaillet B (1997) The redox state of Pinatubo dacite and the ilmenite-hematite solvus. *Am Mineral* 82:625–629
- Fournelle J (1990) Anhydrite in Nevado del Ruiz November 1985 pumice; relevance to the sulfur problem. *J Volcanol Geotherm Res* 42:189–201
- Gerlach TM, Westrich HR, Symonds RB (1996) Preeruption vapor in magma of the climactic Mount Pinatubo eruption: source of the giant stratospheric sulfur dioxide cloud. In: Newhall CG, Punongbayan RS (eds) *Fire and mud: eruptions and lahars of Mount Pinatubo*, Philippines. PHIVOLCS, Quezon City, Philippines and University of Washington Press, Seattle, pp 415–433
- Hattori K (1993) High-sulfur magma, a product of fluid discharge from underlying mafic magma: evidence from Mount Pinatubo, Philippines. *Geology* 21:1083–1086
- Hattori K (1996) Occurrence and origin of sulfide and sulfate in the 1991 Mount Pinatubo eruption products. In: Newhall CG, Punongbayan RS (eds) *Fire and mud: eruptions and lahars of Mount Pinatubo*, Philippines. PHIVOLCS, Quezon City, Philippines and University of Washington Press, Seattle, pp 807–824
- Hattori K, Keith JD (2001) Contribution of mafic melt to porphyry copper mineralization: evidence from Mount Pinatubo, Philippines, and Bingham Canyon, Utah, USA. *Miner Deposita* 26:799–806
- Hattori K, Sato H (1996) Magma evolution recorded in plagioclase zoning in 1991 Pinatubo eruption products. *Am Mineral* 81:982–994
- Holloway JR, Blank JG (1994) Application of experimental results to C–O–H species in natural melts. In: Carroll MR, Holloway JR (eds) *Volatiles in magmas*. *Rev Mineral* 30:187–230
- Imai A, Listanco EL, Fujii T (1993) Petrologic and sulfur isotopic significance of highly oxidized and sulfur-rich magma of Mt. Pinatubo, Philippines. *Geology* 21:699–702
- Ishihara S (1981) The granitoid series and mineralization: economic geology 75th anniversary volume. Society of Economic Geologists, pp 458–484
- Jakubowski RT, Fournelle J, Welch S, Swope RJ, Camus P (2002) Evidence for magmatic vapor deposition of anhydrite prior to the 1991 climactic eruption of Mount Pinatubo, Philippines. *Am Mineral* 87:1029–1045
- Kress V (1997) Magma mixing as a source for Pinatubo sulfur. *Nature* 389:591–593
- Leake BE, Woolley AR, Arps CES, Birch WD, Gilbert MC, Grice JD, Hawthorne FC, Kato A, Kisch HF, Krivovichev VG, Linthout K, Laird J, Mandarino JA, Maresch WV, Nickel EH, Rock NMS, Schumacher JC, Smith DC, Stephen-son NCS, Ungaretti L, Whittaker EJW, Youzhi G (1997) Nomenclature of amphiboles: report of the subcommittee on amphiboles of the International Mineralogical Association, Commission on New Minerals and Mineral Names. *Can Mineral* 35:219–246
- Luhr JF (1990) Experimental phase relations of water- and sulfur-saturated arc magmas and the 1982 eruptions of El Chichón volcano. *J Petrol* 31:1071–1114
- Luhr JF, Melson WG (1996) Mineral and glass compositions in June 15 1991, pumices; evidence for dynamic disequilibrium in the dacite of Mount Pinatubo. In: Newhall CG, Punongbayan RS (eds) *Fire and mud: eruptions and lahars of Mount Pinatubo*, Philippines. PHIVOLCS, Quezon City, Philippines and University of Washington Press, Seattle, pp 733–749
- Luhr JF, Carmichael ISE, Varekamp JC (1984) The 1982 eruptions of El Chichón volcano, Chiapas, Mexico: mineralogy and petrology of the anhydrite phenocryst-bearing pumices. *J Volcanol Geotherm Res* 23:69–108
- Matthews SJ, Jones AP, Bristow CS (1992) A simple magma-mixing model for sulfur behaviour in calc-alkaline volcanic rocks: mineralogical evidence from Mount Pinatubo 1991 eruption. *J Geol Soc Lond* 149:863–866
- Matthews SJ, Jones AP, Gardeweg MC (1994) Lascar volcano, northern Chile; evidence for steady-state disequilibrium. *J Petrol* 35:401–432
- Matthews SJ, Moncrieff DHS, Carroll MR (1999) Empirical calibration of the sulphur valence oxygen barometer from natural and experimental glasses: methods and applications. *Mineral Mag* 63:421–431
- McKibben MA, Eldridge CS, Reyes AG (1992) Multiple origins of anhydrite in Mt. Pinatubo pumice (abstract). *AGU Eos Trans* 73(43):633–634
- McKibben MA, Eldridge CS, Reyes AG (1996) Sulfur isotopic systematics of the June 1991 Mount Pinatubo eruptions: a SHRIMP ion microprobe study. In: Newhall CG, Punongbayan RS (eds) *Fire and mud: eruptions and lahars of Mount Pinatubo*, Philippines. PHIVOLCS, Quezon City, Philippines and University of Washington Press, Seattle, pp 825–843
- Métrich N, Clocchiatti R (1996) Sulfur abundance and its speciation in oxidized alkaline melts. *Geochim Cosmochim Acta* 60:4151–4160
- Métrich N, Bonnín-Mosbah M, Susini J, Menez B, Galois L (2003) Presence of sulfite (S^{IV}) in arc magmas: implications for volcanic sulfur emissions. *Geophys Res Lett* 29/11, doi:10.1029/2001GL014607
- Mungall JE (2002) Roasting the mantle: slab melting and the genesis of major Au and Au-rich Cu deposits. *Geology* 30:915–918
- Newhall CG, Punongbayan RS (1996) *Fire and mud: eruptions and lahars of Mount Pinatubo*, Philippines. PHIVOLCS, Quezon City, Philippines and University of Washington Press, Seattle
- Nilsson K, Peach CL (1993) Sulfur speciation, oxidation state and sulfur concentration in backarc magmas. *Geochim. Cosmochim. Acta* 57:3807–3813
- Pallister JS, Hoblitt RP, Reyes AG (1992) A basalt trigger for the 1991 eruptions of Pinatubo volcano? *Nature* 356:426–428
- Pallister JS, Hoblitt RP, Meeker GP, Knight RJ, Siems DF (1996) Magma mixing at Mount Pinatubo: petrographic and chemical evidence from the 1991 deposits. In: Newhall CG, Punongbayan RS (eds) *Fire and mud: eruptions and lahars of Mount Pinatubo*, Philippines. PHIVOLCS, Quezon City, Philippines and University of Washington Press, Seattle, pp 687–731
- Parkinson JJ, Arculus RJ (1999) The redox state of subduction zones: insights from arc-peridotites. *Chem Geol* 160:409–423
- Poustovetov AA, Roeder PL (2000) The distribution of Cr between basaltic melt and chromium spinel as an oxygen geobarometer. *Can Mineral* 39:309–317
- Rampino MR, Self S (1984) The atmospheric effects of El Chichón. *Sci Am* 250, 48–57
- Roedder E (1984) Fluid Inclusions. *Rev Mineral* 12:644
- Rutherford MJ, Devine JD (1996) Preeruption pressure–temperature conditions and volatiles in the 1991 dacitic magma of Mount Pinatubo. In: Newhall CG, Punongbayan RS (eds) *Fire and mud: eruptions and lahars of Mount Pinatubo*, Philippines. PHIVOLCS, Quezon City, Philippines and University of Washington Press, Seattle, pp 751–766
- Rutherford MJ, Hammer JE (2001) Petrology of the 1991–2 Pinatubo magma system (abstract). *Eos Trans AGU* 82 (47), Fall Meet Suppl Abstract U31A-02
- Scaillet B, Evans BW (1999) The 15 June 1991 eruption of Mount Pinatubo. I. Phase equilibria and pre-eruption P – T – f_{O_2} – f_{H_2O} conditions of the dacite magma. *J Petrol* 40:381–411
- Self S, Zhao J-X, Holasek RE, Torres RC, King AJ (1996) The atmospheric impact of the 1991 Mount Pinatubo eruption. In: Newhall CG, Punongbayan RS (eds) *Fire and mud: eruptions and lahars of Mount Pinatubo*, Philippines. PHIVOLCS, Quezon City, Philippines and University of Washington Press, Seattle, pp 1089–1115
- Sparks SRJ, Sigurdsson H, Wilson L (1977) Magma mixing: a mechanism for triggering acid explosive eruptions. *Nature* 267:315–318
- Wallace PJ (2001) Volcanic SO₂ emissions and the abundance and distribution of exsolved gas in magma bodies. *J Volcanol Geotherm Res* 108:85–106

- Wallace PJ, Carmichael ISE (1992) Sulfur in basaltic magmas. *Geochim Cosmochim Acta* 56:1863–1874
- Wallace PJ, Gerlach TM (1994) Magmatic vapor source for sulfur dioxide released during volcanic eruptions: evidence from Mount Pinatubo. *Science* 265:497–499
- Westrich HR, Gerlach TM (1992) Magmatic gas source for the stratospheric SO₂ cloud from the June 15 1991, eruption of Mount Pinatubo. *Geology* 20:867–870
- Williams SN, Sturchio NC, Calvach V ML, Mendez FR, Londono CA, Garcia PN (1990) Sulfur dioxide from Nevado del Ruiz volcano, Colombia: total flux and isotopic constraints on its origin. *J Volcanol Geotherm Res* 42:53–68
- Yumul GP Jr (1992) Ophiolite-hosted chromitite deposits as tectonic setting and melting degree indicators: examples from the Zambales Ophiolite Complex, Philippines. *Mining geology. J Soc Resour Geol Tokyo* 42:5–17